RSC Advances

PAPER

Cite this: *RSC Adv.*, 2015, **5**, 103834

Atomic-scale cation dynamics in a monolayer VO_X/α-Fe_2O_3 catalyst†

Z. Feng,*[ab] Q. Ma,[c] J. Lu,[dg] H. Feng,[dh] J. W. Elam,[d] P. C. Stair[e] and M. J. Bedzyk*[af]

Received 9th September 2015
Accepted 16th November 2015

DOI: 10.1039/c5ra18404e

www.rsc.org/advances

Catalytic reactions are associated with dynamical changes in the catalyst that include the oxidation state and local structural variations. The understanding of such dynamics, particularly at the atomic-scale, is of great importance for revealing the activity and selectivity of the catalyst in numerous reactions. Combining *in situ* X-ray absorption spectroscopy with *in situ* diffuse reflectance infrared Fourier transform spectroscopy, we studied the redox-induced dynamical changes for a VO_X monolayer catalyst supported on a α-Fe_2O_3 powder. The results show that several co-existing VO_X species reversibly change their V oxidation states between +5 and +4, in concurrence with a structural change from two-dimensional chains to well connected V–O–V networks. These changes are also associated with the breaking and formation of the V=O vanadyl group. This combined study provides new insight into how VO_X species change during catalytic reactions, which leads to proposed atomic-scale models for the redox-induced dynamics of the catalyst.

1. Introduction

Heterogeneous catalysts, due to their high activity and selectivity, are crucial for industrial, environmental and energy applications[1] such as petroleum refining,[2] the selective catalytic reduction of automotive and industrial NO_X emissions,[3] and fuel cells.[4–6] It has been known that catalysts go through dynamical changes (*i.e.* geometric structure, chemical and electronic structure) during chemical reactions, which, however, are difficult to observe directly. The activity of a catalyst is strongly linked to its structure and the strategic hosting arrangements provided by the support.[7,8] By proper choice of key catalytic elements and their host structures, preferred reaction pathways can be selected over less desired ones. Therefore, it is important to understand the atomic-scale structures as well as the surface chemistry of catalysts, and consequently the catalytic reaction mechanisms for tuning catalytic properties.

Supported vanadium oxides (VO_X) are of great interest scientifically and for industrial applications due to their rich and diverse chemistry,[9] and their potential for catalyzing a number of oxidation reactions, *e.g.*, the oxidation of methanol to formaldehyde and the oxidative dehydrogenation of light alkanes.[10–13] Various parameters have been shown to affect the catalytic properties of VO_X catalysts, for example, vanadium oxide loading, molecular structure, electronic structure and the nature of the supporting oxide.[14,15] Although many researchers have investigated the activity and selectivity of VO_X, little is known about the details of their atomic structure and its transformation during the catalytic cycle and how this contributes to their catalytic action.[16] In particular, hematite (α-Fe_2O_3) supported VO_X is a widely used catalyst.[17] However, the effect of the atomic structures of VO_X on the catalytic properties are unknown. A key aspect of these questions is a knowledge of how the VO_X is anchored to the surface of the support materials under reaction conditions.[18] Although the structure of VO_X in the oxidized form has been studied extensively, there remains significant debate. In contrast, the structure of the reduced VO_X species is essentially unknown. This absence of detailed structural information makes it difficult to establish the relationships between the atomic structure, composition, electronic properties, and the resulting catalytic performance.[19] In this regard, we chose X-ray absorption spectroscopy (XAS), which is capable of probing, *in situ*, the influence of the local environment on the properties of the catalytically active species.[20] The oxidation states and atomic-

[a]*Department of Materials Science and Engineering, Northwestern University, Evanston, IL, 60208, USA. E-mail: z-feng@u.northwestern.edu; bedzyk@northwestern.edu*

[b]*Chemical Sciences and Engineering Division, Argonne National Laboratory, Lemont, IL, 60439, USA*

[c]*DND-CAT, Synchrotron Research Center, Northwestern University, Evanston, IL, 60208, USA*

[d]*Energy Systems Division, Argonne National Laboratory, Lemont, IL, 60439, USA*

[e]*Department of Chemistry, Northwestern University, Evanston, IL, 60208, USA*

[f]*Department of Physics and Astronomy, Northwestern University, Evanston, IL, 60208, USA*

[g]*Department of Chemical Physics, University of Science and Technology of China, Jinzhai Road 96#, Baohe District, Hefei, 230026, China*

[h]*Xi'an Modern Chemistry Research Institute, 168 E. Zhangba Road, Xi'an, Shaanxi, 710065, China*

† Electronic supplementary information (ESI) available: Details about the XANES linear fits, EXAFS analysis for determination of the second shell and bond assignment. See DOI: 10.1039/c5ra18404e

structural information can be extracted from X-ray absorption near edge structure (XANES) and extended X-ray absorption fine structure (EXAFS), respectively. However, spectroscopic and structural studies of oxidation catalysts under reaction conditions only provide information on the most abundant surface species, typically in the oxidized state. When the catalytic cycle can be broken up into two half cycles corresponding to reduction and reoxidation, it is possible to trap the catalyst in its reduced state and perform detailed structural and spectroscopic measurements. This strategy is employed in the present paper.

Our previous studies[21–24] for monolayer (ML) vanadium oxides supported on oxide single crystal surfaces have shown the structural dynamics of vanadium cations as the oxidation state cycles between V^{3+}/V^{4+} and V^{5+}. Observations of chemical and structural transformations and coherence of supported catalyst under redox cycling can provide information on the structure of active sites and the reversibility of the reaction. Typically there is a materials gap between the model single crystal and real catalytic systems. Therefore, the current work is focused on polycrystalline materials, as they are real catalysts used in practical chemical transformations.[25] Although the impregnation method is the most common way to prepare catalysts, to simplify the study we chose atomic-layer deposition (ALD) and used H_2 and O_2 for the reduction and oxidization of VO_X, respectively, to mimic the real reactions. The obtained insights will have a direct and practical impact on the development of many industrial processes.

Herein, we study an ML VO_X catalyst on α-Fe_2O_3 powder. ALD is chosen compared to other conventional methods such as sol–gel because catalyst can be coated homogenously on the irregular surfaces of powder materials. During reduction–oxidation (redox) reaction cycles, *in situ* XAS is used to gain information on the oxidation states of VO_X species and their atomic-structures. With the combination of *in situ* diffuse reflectance infrared Fourier transform spectroscopy (DRIFTS), we observed the corresponding changes of VO_X molecular structure. This first combined study on VO_X/α-Fe_2O_3 provides insights of how vanadium oxides transform chemically and structurally in redox reactions and their role in the reaction mechanism.

2. Experiment

2.1 Sample preparation

Commercial high purity (99%) α-Fe_2O_3 (hematite) powders were purchased from Alfa Aesar as substrates. ALD was carried out at 200 °C in a viscous flow reactor[26] and ultra high purity nitrogen (Airgas, 99.999%) was used as the purge gas. For the growth of VO_X, the substrates were exposed first to vanadium oxytriisopropoxide (VOTP, Sigma Aldrich), at a partial pressure of 0.05 Torr for 200 s, followed by a nitrogen purge for 100 s. The substrates were then exposed to hydrogen peroxide at a partial pressure of 0.2 Torr for 200 s, followed by a nitrogen purge for 100 s (200–100–200–100 s). This process is defined as one ALD cycle. 5 ALD cycles of vanadium oxide were used to coat the hematite substrates. The substrate surface area was measured to be 6 $m^2\ g^{-1}$ by the Brunauer, Emmett and Teller method, and the sample weight gain after ALD was ~0.7%. Therefore the VOx coverage can be estimated to be 1.4 ML, where 1 ML is defined as 10 V atoms per nm^2 (see eqn (S1) in ESI† for details).

2.2 *In situ* XAS measurements

In situ XAS experiments were carried out at beamline 5BM-D of the DuPont-Northwestern-Dow Collaborative Access Team (DND-CAT) at the Advanced Photon Source (APS) of Argonne National Laboratory (ANL). 10 mg of VO_X/α-Fe_2O_3 powder was mixed evenly with 190 mg boron nitride (BN) powder, and the mixture was pressed as a wafer. The pellet was mounted into a custom *in situ* XAS cell.[27,28] The cell consisted of two concentric cylinders with Kapton windows at the ends and a thermocouple port for internal temperature measurement just downstream of the sample. Gas entered *via* the outer cylinder, swept through the region between the cylinders, and exited from the inner cylinder after passing through the self-supporting wafer, which was mounted at the gas inlet of the inner cylinder. All data were collected in fluorescence mode under controlled temperature and gas environment. A 13-element solid state Ge detector was used to collect the vanadium(v) and iron (Fe) K fluorescence signals while the Si(111) monochromator scanned the incident X-ray photon energy through the V and Fe K absorption edges. The monochromator was detuned to 65% of the maximum intensity at the V K-edge (5465 eV) and Fe K edge (7112 eV) to minimize higher harmonics. XAS measurements were performed at each step of the redox reaction process; namely as-deposited (AD), oxidized (OX), reduced (RE) and re-oxidized (OX2) conditions. The oxidized and reduced samples were prepared by annealing at 270 °C for 30 min in pure O_2 and 350 °C for 30 min in 3% H_2 balanced with helium gas, respectively. The re-oxidized surfaces were prepared by annealing at 350 °C for 30 min in O_2 condition to ensure complete oxidation of the VO_X. All spectra were collected after cooling to room temperature in ultrahigh purity (99.999%) helium with a flow rate of 100 sccm. Reference samples of V_2O_5 and VO_2 from Sigma-Aldrich were measured in transmission mode. The V and Fe edge energies were calibrated using the V and Fe metal foils, respectively.

Data reduction and analysis were performed with the Athena, Artemis and IFEFFIT software packages.[29] Standard procedures were used to extract the EXAFS data from the measured absorption spectra. The pre-edge was linearly fitted and subtracted. The post-edge background was determined by using a cubic-spline-fit procedure and then subtracted. The data were normalized by the height of the absorption edge. For quantitative analyses, phase shifts and back-scattering amplitudes were generated by the FEFF calculations based on crystalline structures, namely, V_2O_5 and VO_2, and were then calibrated through performing the FEFFIT of reference samples' EXAFS data, mainly to obtain the amplitude reduction factor S_0^2. With the known S_0^2, the EXAFS data of the samples were fitted with such generated phase shifts and amplitudes. Accuracies of obtained results presented here are: N (±10%), R (±1%), $\Delta\sigma^2$ (±10%) and ΔE_0 (±10%).[30,31]

2.3 *In situ* DRIFT measurements

In situ DRIFTS measurements were performed at room temperature after each redox reaction process using a Thermo Nicolet Nexus 870 instrument with a Mercury-Cadmium-Telluride detector (Keck II facility at Northwestern University). The background spectra were taken on the hematite powder after calcination at 200 °C for 20 min in 10% oxygen in helium, and cooling back to room temperature in ultrahigh purity (99.999%) helium at a flow rate of 100 sccm. The ALD VO_X/hematite sample was then loaded into the DRIFTS cell to perform the redox reactions and collect spectra. The oxidation was carried out in 10% oxygen in helium at a flow rate of 100 sccm at 350 °C for 20 min. The reduction was performed at in 5% H_2 balanced with nitrogen at 350 °C for 10 min. Except for the spectrum that was collected in the H_2 flowing gas after ~5 minute purging, all the other spectra were collected after cooling to room temperature in helium (512 scans, a resolution of 4 cm^{-1}). Although the oxygen and hydrogen percentages were not exactly the same as those used for XAS measurements, the oxidation and reduction time is long enough to ensure that VO_X species were fully oxidized or reduced.

3. Results and discussion

The normalized XANES spectra of VO_X/hematite at the AD, OX, RE and OX2 conditions are plotted in Fig. 1a. Comparison to the spectra from the V_2O_5 and VO_2 references clearly shows that hematite supported vanadium oxides go reversibly from V^{5+} in the oxidized state to V^{4+} in the reduced state. Careful examination shows that the OX pre-peak width is larger than that of bulk V_2O_5, and its rising edge has a ~0.7 eV shift towards lower energy compared to that of V_2O_5, but with the same slope as that of either RE or VO_2. This suggests that the OX sample may contain some fraction of V^{4+}. A fit of the OX XANES using a linear combination of VO_2 and V_2O_5 reference spectra gives an estimated 10% V^{4+} in the OX, while the line shape analysis of the OX XANES gives an estimate of 6% V^{4+} in the sample (see Fig. S1 in ESI† for details). In addition, the XANES of VO_X/hematite are rather different from those of the references, suggesting that the local structures around V may deviate from those of bulk V_2O_5 and VO_2. The change of the pre-peak intensity (Fig. 1a) is indicative of the changes in the local symmetry around V, namely the lower the symmetry, the higher the pre-peak intensity.[32] For bulk V_2O_5 that forms an orthorhombic (*Pmmn*) layer crystal,[33] each vanadium atom and its five nearest oxygen neighbors create an edge- and corner-share distorted VO_5-pyramid with one short V=O bond of 1.58 Å and four V–O bonds of 1.83 Å.[14] In contrast, for bulk VO_2 (either rutile or monoclinic), each vanadium atom is surrounded by six oxygen atoms to form a distorted VO_6 octahedral structure with V–O distances in the range 1.76–1.87 and 2.01–2.05 Å.[9,34] Therefore, V_2O_5 that has lower local symmetry around V shows more pronounced pre-peak intensity. It is also noted that the oxidized VO_X/hematite has higher pre-peak intensity compared to that in RE (Fig. 1b) and VO_2, thus a lower local symmetry around V is expected. The ratio of the pre-peak height (H) to the edge-jump height (S) can be used to determine the local symmetry. For a perfect tetrahedron this value is 0.8–1.0.[30] In our case, the H/S ratio of the OX is ~0.55, suggesting a possible distorted tetrahedral local structure, while the H/S ratio in RE is reduced to ~0.3 in RE, suggesting an octahedrally coordinated geometry, which is supported by the nearly identical pre-peaks of VO_2 and VO_X in RE (Fig. 1a).

Further experiments also indicate that the complete reduction of V^{5+} to V^{4+} can only be realized above 350 °C, and temperatures below that only lead to the partial reduction of V^{5+}, as shown in Fig. 1b. Similarly, the oxidation from V^{4+} to V^{5+} also has to be performed above 350 °C. Note that the temperature-dependent XANES measurements were done in the H_2 or O_2 condition. Thermodynamically there is no equilibrium between oxidized and reduced VO_X. Furthermore, the XANES pre-edges of the OX and OX2 do not exactly overlap with that of V_2O_5 (Fig. 1a). These results imply the existence of various VO_X species that have different energy barriers for redox reactions and these VO_X species could be a mixture of V^{4+} and V^{5+}, instead of gradual reduction or oxidization of the same VO_X species. This hypothesis is further supported by previous Raman and theoretical studies of θ-Al_2O_3 supported VO_X,[35,36] which suggested that the co-existence of several VO_X species can lead to different catalytic reduction temperatures. As these VO_X species have similar local atomic structures, they are hard to distinguish by XAS.

The change between V^{4+} and V^{5+} for the reduced and oxidized VO_X, respectively, has been observed in our previous model system studies on VO_X/α-TiO_2(110), which suggests that V alters its oxidation state between 4+ and 5+ if V coverage is more than 1 ML, while between 3+ and 5+ if the coverage is less than 1 ML.[13,22,24] This study on powder VO_X is consistent with our studies on model system. This may be due to the high

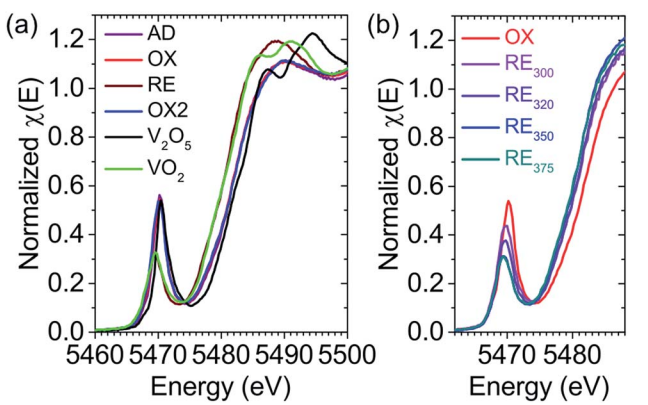

Fig. 1 (a) Normalized V K-edge XANES spectra for VO_X/α-Fe_2O_3 in as-deposited (AD, purple), oxidized (OX, red), reduced (RE, violet) and re-oxidized (OX2, blue) conditions and comparisons with V_2O_5 (black) and VO_2 (green) powder references. Clearly OX and OX2 spectra are overlapped, suggesting the reversible changes on VO_X catalyst. (b) The comparison of pre-edge peak intensities of VO_X/α-Fe_2O_3 reduced at different temperatures. RE_{300}, RE_{320}, RE_{350}, and RE_{375} denote the reduction temperatures of 300 °C, 320 °C, 350 °C, and 375 °C, respectively.

energy barrier for high coverage VO_X to be reduced to V^{3+}, which needs future theoretical investigation.

The Fe K edge XANES and EXAFS for AD, OX, RE and OX2 were measured correspondingly (Fig. S2†). However, no change for Fe was found during the redox. This could also be due to bulk-sensitive XAS that cannot detect the surface changes of Fe_2O_3, in our case, where only ~3% of the Fe is surface Fe in the Fe_2O_3 particles with average size of 5 μm. At 350 °C, surface Fe^{3+} cations are possibly reduced due to low V coverage and/or well dispersed V species to assist the reduction of V, as observed in our previous studies of VO_X on single crystal α-Fe_2O_3(0001).[23] Future experiments can be designed to work with α-Fe_2O_3 nanoparticles (*i.e.*, <10 nm), for which signals from surface Fe dominate.

The change in the local atomic structure around V cations is extracted from the V K edge EXAFS data collected at each redox-processing step. Fig. 2 shows the Fourier transforms of the EXAFS spectra collected for one redox cycle (OX-RE-OX2), and are compared to those of bulk VO_2 and V_2O_5. The OX2 EXAFS is similar to that of the OX indicating reversibility, which is in agreement with the XANES measurements (also see Fig. S3† for comparison of data in *k* space). The distinct spectra for RE and OX suggest that these supported vanadium oxides have different atomic structures, and differ markedly from their corresponding bulk references. Using the amplitude reduction factor, $S_0^2 = 0.65$, obtained from the fit of the V_2O_5 reference (Fig. S4†), the first neighbor structure around V in the OX sample is best reproduced by 2.2 V–O bonds of 1.62 Å and 1.7 V–O bonds of 1.82 Å (Table 1), suggesting a total coordination number $N = 4$. The small Debye–Waller factor, σ^2 ($<10^{-3}$ Å^2 compared to 5.7×10^{-3} from V_2O_5 analysis), may be indicative of somewhat underestimated value of N, given the strong correlation between σ^2 and N. However, the large H/S ratio of ~0.55 for the OX VO_X indicates a dominant low symmetry coordination configuration around V.

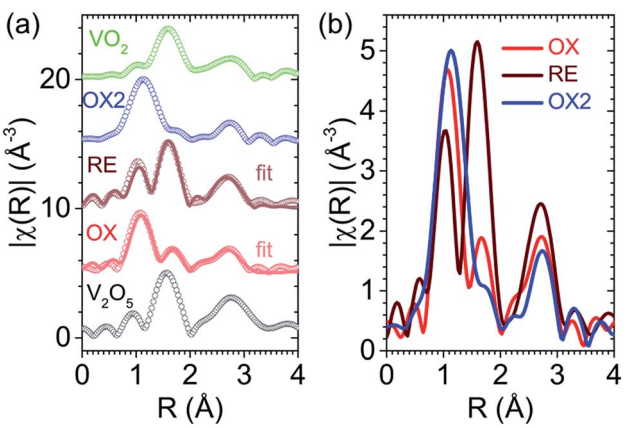

Fig. 2 (a) Fourier transforms (FT) of vanadium K-edge EXAFS spectra (open circles) for V_2O_5 (black) and VO_2 (green) reference powders, and VO_X/α-Fe_2O_3 in oxidized (OX, red), reduced (RE, wine) and re-oxidized (OX2, blue) conditions. The lighter-colored lines are fits to the EXAFS data for VO_X/α-Fe_2O_3 in OX and RE conditions. Data are offset vertically for clarity. (b) EXAFS FT for OX, RE and OX2 show big differences between the oxidized and reduced state for VO_X, but similarity in peak positions and amplitudes between OX and OX2, suggesting the reversibility of this redox reaction.

Table 1 Summary of EXAFS fitting results for the oxidized (OX) and reduced (RE) samples. The detailed bond assignments for a VO_4 tetrahedral unit in OX and a VO_6 octahedral unit in RE are descripted in Fig. S5 of ESI

Condition	Scattering pair	*N*	*R* (Å)	σ^2 (Å^2)
OX	$V–O_{(1)}$	2.2	1.62	0.0007
	$V–O_{(2)}$	1.7	1.82	0.0009
	V⋯Fe	2.0	3.03	0.0090
RE	$V–O_{(1)}$	2.0	1.66	0.0057
	$V–O_{(2)}$	5.4	1.96	0.0075
	V⋯Fe	2.7	3.02	0.0070

Previous studies[14,37–40] have suggested that oxide-supported VO_X in a V^{5+} oxidation state has a VO_4 tetrahedral structure with one V=O bond, one V–O–$M_{support}$ bond (M represents the support metal cation) and two V–O–V bonds. Although EXAFS studies[30,41–44] of vanadium oxides on different supports suggested that the VO_4 unit has one V=O bond ~1.6 Å and multiple V–O bonds ~1.8 Å, our study shows that the OX contains VO_4 tetrahedral units with two short V–O bonds. To the best of our knowledge, this is the first structural study of VO_X anchored on polycrystalline Fe_2O_3. The different VO_X atomic structures compared to previous studies of VO_X on other supports (*e.g.*, SiO_2, TiO_2, ZrO_2) could be due to the interaction between VO_X and Fe_2O_3 surface to minimize the surface energy. It is interesting to note that the VO_4 unit in bulk $Fe_2V_4O_{13}$ also has two short vanadium–oxygen bonds (~1.6 Å) and two long vanadium–oxygen bonds (~1.8 Å).[45] One of the short bonds is V–O in either V–O–V or V–O–Fe geometry. Therefore, the 1.62 Å bonds from our EXAFS analysis are assigned to a V=O bond and a V–O bond in either V–O–V or V–O–Fe geometry, while accordingly the larger bond of 1.82 Å is assigned to V–O bonds in either V–O–V or V–O–Fe, respectively (see Fig. S5†).

Similarly, the analysis of the RE sample gives *ca.* 2 V–O bonds of 1.66 Å and *ca.* 5 V–O bonds of 1.96 Å, with $\sigma^2 = 5.7 \times 10^{-3}$ and $\sigma^2 = 7.5 \times 10^{-3}$ Å^2, respectively. The short V–O bond is considerably shorter than the shortest bond (1.76 Å) in bulk VO_2, while the long V–O bond is close to the weight-averaged bond length (1.93 Å) in VO_2. Given the large error in the coordination number and the excellent overlap of the V XANES spectra for RE and the VO_2 reference, a distorted octahedral coordination geometry around V is proposed. Such a VO_6 local structure forms V–O–V networks, which were also found in our pervious study of ML VO_X supported on α-TiO_2(110) single crystal.[13] As there are two different cases for VO_X in OX, there can be three different bonding structures with 1.66 Å for either V–O bonds from V–O–Fe and/or 1.96 Å to the long V–O bonds from V–O–V (see Fig. S5†).

Analysis of the second shell at ~3 Å in Fig. 2 is complicated, but the results show that 3.03 Å and 3.02 Å can be assigned to V⋯Fe bonds in V–O–Fe for OX and RE, respectively, where the symbol "⋯" implies that the V and Fe are next-nearest-neighbors (see Fig. S6 and S7, and ESI† for details). This is

consistent with V···$M_{support}$ distances for VO_X supported on various substrates, *e.g.* SiO_2, ZrO_2 and Nb_2O_5.[30,46] Since the Fe–O bond in bulk α-Fe_2O_3 is 1.91 Å, in the triangle that is made of V, O, and Fe, the V–O–Fe bond angle can be calculated to be 118° (V–O bond 1.62 Å) or 111° (V–O bond 1.82 Å), which is slightly larger than 101° of V–O–$Si_{support}$[46] but smaller than most V–O–M bond angles in vanadium compounds that range from 128° to 155° (ref. 47) (see Fig. S5 in ESI† for detailed bond assignments).

To further understand the reversible structural and chemical transformation of V cations during redox reactions, *in situ* DRIFTS was performed. Fig. 3 shows the *in situ* background-subtracted DRIFTS measurements on VO_X/hematite powder at different redox processing steps. Changes in the V bonding configuration are clearly seen when comparing AD, OX, RE, and OX2. Additional differences appeared when the measurements were performed in flowing H_2 and after reduction/oxidation at different temperatures. The peaks around 1030 cm^{-1} are assigned to the V=O stretch.[39,48–50] For the AD sample, there are 3 V=O related peaks that can be attributed to different V=O bond types influenced by varying degrees of hydration. After the first oxidation, there is only one dominant V=O stretching band at 1034 cm^{-1}, which is a consequence of dehydration.[39,49,51] The V=O feature is also evidence for V^{5+}. During the flow of 5% H_2 balanced with nitrogen at room temperature, the V=O peak intensity was reduced and the position shifted slightly to lower wavenumbers. This is likely due to partial hydration of the V=O bonds by residual moisture in the H_2 line, because an increase in the water background was clearly observed in the difference spectrum between the spectra of OX and H_2 flow (not shown here). Upon heating to 300 °C in 5% H_2 in N_2, the V=O peak intensity was diminished, which indicates V reduction. Meanwhile, new peaks appeared at 890 cm^{-1} and 1100 cm^{-1}, which can be assigned to the V–O–V stretching mode in polymeric VO_X species[48,50] and the overtone of V–O–V bonds at 550 cm^{-1},[52] respectively. However, reduction of V cations was incomplete until the reduction temperature was increased to 350 °C, at which point the peaks at 890 cm^{-1} and 1103 cm^{-1} became more pronounced and the V=O peak at 1030 cm^{-1} completely disappeared. This behavior is consistent with the XAS measurements that 350 °C is the temperature required for complete VO_X/hematite reduction. H_2 reduction eliminates the V=O stretch band, indicating a dramatic change in the VO_X structure and oxidation state. The increase of the V–O–V absorbance peak suggests an aggregation of polymeric VO_X species. This is also consistent with XAS measurements. Similarly, complete oxidation (OX2) requires temperatures above 350 °C. The reappearance of the V=O stretching mode and the disappearance of the V–O–V stretching mode agree with the oxidation of V^{4+} to V^{5+} as well as the structural reversibility found in XANES and EXAFS measurements. The observation here of vanadyl bond reduction by a reducing gas such as H_2 at high temperature is consistent with that in previous studies,[10,53] which have shown that the reactivity of VO_X catalysts in redox reactions is closely correlated with the reducibility of the vanadyl group. However, the present work demonstrates that significant structural changes accompany the oxidation state change, in addition to a simple breaking and formation of the vandyl oxygen bond. Although the FTIR results are similar to what was observed previously for cyclohexane oxidative dehydrogenation on single crystal α-TiO_2(110) supported VO_X, the present work provides the chemical, atomic, and bonding structures of VO_X in both the OX and RE conditions on a polycrystalline support with sufficient surface area for catalytic activity tests and possible practical applications.

Based on information gained from *in situ* XAS and *in situ* FTIR, we propose the schematic models depicted in Fig. 4 to explain the transformations of VO_X/hematite during H_2/O_2 redox reactions. This models shows how surface VO_X alters its

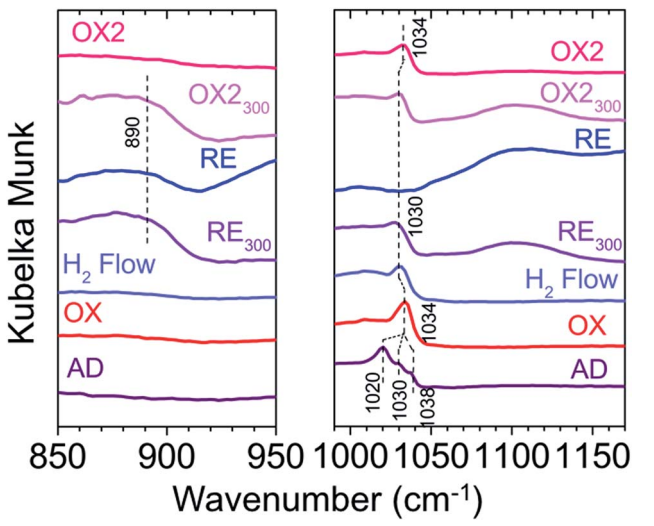

Fig. 3 *In situ* DRIFTS measurements of VO_X supported on hematite α-Fe_2O_3 powder after sequential oxidation and reduction using O_2 and H_2, respectively. The wavenumber regions, shown on the left- and right-hand sides, are from the same individual infrared spectra collected after each treatment step but with different offsets for clarity. RE_{300} and $OX2_{300}$ denote the reduction and re-oxidation temperatures at 300 °C, respectively. The OX2 data at the very top is for re-oxidation performed at 350 °C.

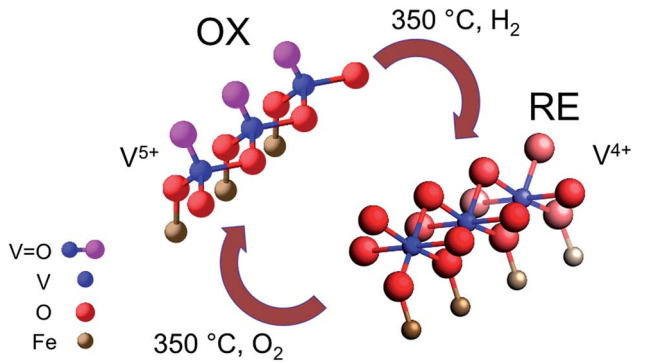

Fig. 4 Perspective view of models for redox reaction on hematite (α-Fe_2O_3) supported ML VO_X. In the oxidized (OX) condition, V^{5+} with tetrahedral VO_4 structure is bonded to the α-Fe_2O_3 surface with one V=O, one V–O–Fe, and two V–O–V bonds in each unit. In the reduced (RE) state, V^{4+} in an octahedral VO_6 network are formed. During H_2 reduction, V=O bonds are broken and converted to V–O–V and V–O–Fe linkages.

oxidation state, bonding, and atomic structure. Oxidation results in tetrahedral VO_4 structures, which are bound to hematite surfaces with one V–O–Fe for each VO_4 unit, forming two-dimensional chains similar to the polymeric vanadium oxides anchored on oxide surfaces described by Weckhuysen *et al.*[14] H_2 molecules interact with the V=O bonds from V^{5+} in the OX state, reducing the vanadium oxides. This reduction not only changes V^{5+} to V^{4+}, but also causes the transformation from a corner-shared tetrahedral VO_4 structure to a highly interactive edge-shared VO_6 network. More V–O–V and V–O–Fe linkages are created. Our studies also found that temperature is critical for catalysts to become activated, *i.e.* to achieve complete oxidization or reduction during redox reactions. Compared to our previous study of VO_X on both single crystals[21–24] and powdered rutile,[13] VO_X supported on hematite powder shows better reversibility in both oxidation state and atomic structure. This could be due to a stronger interaction between VO_X and the hematite substrate, which assists the VO_X in catalytic oxidation reactions.

4. Conclusion

In summary, we have combined *in situ* XAS and DRIFTS to study the transformation of ML VO_X on hematite powder surfaces in redox reactions. Using *in situ* XAS, we directly witnessed the catalysts' surface dynamics during reaction, and observed the temperature-dependent changes associated with the reaction energy barrier. *In situ* DRIFTS shows that upon reduction, the V=O bond is broken and the V–O–V network is strengthened. Our measurements not only demonstrate that the vanadyl bond is the critical participant, but also revealed that the V oxidation state changes together with local atomic structural rearrangements. This can be explained by the Mars-van Krevelen reaction mechanism and in our case V cations change from V^{5+} to V^{4+}, concurrent with the transformation of VO_4 tetrahedra to VO_6 octahedra between the oxidized and reduced states. All changes are reversible, suggesting a good reversibility of V catalysts. This combined-technique strategy has important implications for understanding a range of catalytic reactions on powder catalysts that are widely used commercially. Our next step is to further implement catalytic tests into our experiments to associate structural changes with catalysts' activity and selectivity. Knowledge of the structural and oxidation state transformations under real catalytic conditions will provide both atomic-scale and macroscopic views of the structure–activity relationships.

Acknowledgements

This work was supported by the Institute for Catalysis in Energy Processes (DOE Grant DE-FG02-03ER15457). X-ray measurements were performed at APS Sector 5 (DND-CAT) located at ANL, which is supported by DOE Grant DE-AC02-06CH11357. DND-CAT is supported by through E. I. duPont de Nemours & Co., Northwestern University, Dow Chemical Co., the State of Illinois through the Department of Commerce and the Board of Education (HECA), and the US National Science Foundation. JL and JWE were supported as part of the Institute for Atom-efficient Chemical Transformations, an Energy Frontier Research Center funded by DOE, Office of Science, Office of Basic Energy Sciences. The XPS and DRIFTS measurements used the Keck-II facility at Northwestern University. Authors thank Prof. Harold H. Kung of Northwestern University for providing the *in situ* XAS cell. This work made use of NU Central Facilities supported by the MRSEC through NSF Contract No. DMR-1121262.

Notes and references

1 S. M. George, *Chem. Rev.*, 1995, **95**, 475–476.
2 D. H. Park, S. S. Kim, H. Wang, T. J. Pinnavaia, M. C. Papapetrou, A. A. Lappas and K. S. Triantafyllidis, *Angew. Chem., Int. Ed.*, 2009, **48**, 7645–7648.
3 J. Banas, M. Najbar and V. Tomasic, *Catal. Today*, 2008, **137**, 267–272.
4 Z. Feng, Y. Yacoby, W. T. Hong, H. Zhou, M. D. Biegalski, H. M. Christen and Y. Shao-Horn, *Energy Environ. Sci.*, 2014, **7**, 1166–1174.
5 Z. Feng, Y. Yacoby, M. J. Gadre, Y. L. Lee, W. T. Hong, H. Zhou, M. D. Biegalski, H. M. Christen, S. B. Adler, D. Morgan and Y. Shao-Horn, *J. Phys. Chem. Lett.*, 2014, **5**, 1027–1034.
6 J. K. Norskov, T. Bligaard, J. Rossmeisl and C. H. Christensen, *Nat. Chem.*, 2009, **1**, 37–46.
7 O. Bondarchuk, X. Huang, J. Kim, B. D. Kay, L. S. Wang, J. M. White and Z. Dohnalek, *Angew. Chem., Int. Ed.*, 2006, **45**, 4786–4789.
8 Y. K. Kim, Z. Dohnalek, B. D. Kay and R. Rousseau, *J. Phys. Chem. C*, 2009, **113**, 9721–9730.
9 S. Surnev, M. G. Ramsey and F. P. Netzer, *Prog. Surf. Sci.*, 2003, **73**, 117–165.
10 A. Khodakov, B. Olthof, A. T. Bell and E. Iglesia, *J. Catal.*, 1999, **181**, 205–216.
11 G. Deo and I. E. Wachs, *J. Catal.*, 1994, **146**, 323–334.
12 B. Kilos, A. T. Bell and E. Iglesia, *J. Phys. Chem. C*, 2009, **113**, 2830–2836.
13 Z. Feng, J. L. Lu, H. Feng, P. C. Stair, J. W. Elam and M. J. Bedzyk, *J. Phys. Chem. Lett.*, 2013, **4**, 285–291.
14 B. M. Weckhuysen and D. E. Keller, *Catal. Today*, 2003, **78**, 25–46.
15 G. Deo and I. E. Wachs, *J. Phys. Chem.*, 1991, **95**, 5889–5895.
16 F. A. Grant, *Rev. Mod. Phys.*, 1959, **31**, 646–674.
17 H. S. Oliverira, L. C. A. Oliverira, M. C. Pereira, J. D. Ardisson, P. P. Souza, P. O. Patricio and F. C. C. Moura, *New J. Chem.*, 2015, **39**, 3051–3058.
18 U. Diebold, *Appl. Phys. A: Mater. Sci. Process.*, 2003, **76**, 681–687.
19 D. W. Goodman, *Chem. Rev.*, 1995, **95**, 523–536.
20 R. J. Lad and V. E. Henrich, *Surf. Sci.*, 1988, **193**, 81–93.
21 C. Y. Kim, J. W. Elam, P. C. Stair and M. J. Bedzyk, *J. Phys. Chem. C*, 2010, **114**, 19723–19726.
22 Z. Feng, L. Cheng, C.-Y. Kim, J. W. Elam, Z. Zhang, L. A. Curtiss, P. Zapol and M. J. Bedzyk, *J. Phys. Chem. Lett.*, 2012, **3**, 2845–2850.
23 C. Y. Kim, A. A. Escuadro, P. C. Stair and M. J. Bedzyk, *J. Phys. Chem. C*, 2007, **111**, 1874–1877.

24 Z. Feng, M. E. McBriarty, A. U. Mane, J. Lu, P. C. Stair, J. W. Elam and M. J. Bedzyk, *RSC Adv.*, 2014, **4**, 64608–64616.
25 C. Milone, R. Ingoglia, A. Pistone, G. Neri, F. Frusteri and S. Galvagno, *J. Catal.*, 2004, **222**, 348–356.
26 J. W. Elam, M. D. Groner and S. M. George, *Rev. Sci. Instrum.*, 2002, **73**, 2981–2987.
27 J. H. Yang, J. D. Henao, C. Costello, M. C. Kung, H. H. Kung, J. T. Miller, A. J. Kropf, J. G. Kim, J. R. Regalbuto, M. T. Bore, H. N. Pham, A. K. Datye, J. D. Laeger and K. Kharas, *Appl. Catal., A*, 2005, **291**, 73–84.
28 S. M. Oxford, J. D. Henao, J. H. Yang, M. C. Kung and H. H. Kung, *Appl. Catal., A*, 2008, **339**, 180–186.
29 B. Ravel and M. Newville, *J. Synchrotron Radiat.*, 2005, **12**, 537–541.
30 D. E. Keller, D. C. Koningsberger and B. M. Weckhuysen, *Phys. Chem. Chem. Phys.*, 2006, **8**, 4814–4824.
31 G. G. Li, F. Bridges and C. H. Booth, *Phys. Rev. B: Condens. Matter Mater. Phys.*, 1995, **52**, 6332–6348.
32 T. E. Westre, P. Kennepohl, J. G. de Witt, B. Hedman, K. O. Hodgson and E. I. Solomon, *J. Am. Chem. Soc.*, 1997, **119**, 6297–6314.
33 A. Michalak, M. Witko and K. Hermann, *Surf. Sci.*, 1997, **375**, 385–394.
34 T. Yao, X. D. Zhang, Z. H. Sun, S. J. Liu, Y. Y. Huang, Y. Xie, C. Z. Wu, X. Yuan, W. Q. Zhang, Z. Y. Wu, G. Q. Pan, F. C. Hu, L. H. Wu, Q. H. Liu and S. Q. Wei, *Phys. Rev. Lett.*, 2010, **105**, 226405.
35 H. S. Kim, S. A. Zygmunt, P. C. Stair, P. Zapol and L. A. Curtiss, *J. Phys. Chem. C*, 2009, **113**, 8836–8843.
36 H. Kim, G. A. Ferguson, L. Cheng, S. A. Zygmunt, P. C. Stair and L. A. Curtiss, *J. Phys. Chem. C*, 2012, **116**, 2927–2932.
37 I. E. Wachs and B. M. Weckhuysen, *Appl. Catal., A*, 1997, **157**, 67–90.
38 P. R. Shah, J. M. Vohs and R. J. Gorte, *Catal. Lett.*, 2008, **125**, 1–7.
39 S. L. Wegener, H. Kim, T. J. Marks and P. C. Stair, *J. Phys. Chem. Lett.*, 2011, **2**, 170–175.
40 V. Shapovalov and H. Metiu, *J. Phys. Chem. C*, 2007, **111**, 14179–14188.
41 G. Silversmit, H. Poelman, I. Sack, G. Buyle, G. B. Marin and R. de Gryse, *Catal. Lett.*, 2006, **107**, 61–71.
42 J. Wong, F. W. Lytle, R. P. Messmer and D. H. Maylotte, *Phys. Rev. B: Condens. Matter Mater. Phys.*, 1984, **30**, 5596–5610.
43 N. G. Condon, F. M. Leibsle, A. R. Lennie, P. W. Murray, D. J. Vaughan and G. Thornton, *Phys. Rev. Lett.*, 1995, **75**, 1961–1964.
44 J. Haber, A. Kozlowska and R. Kozlowski, *J. Catal.*, 1986, **102**, 52–63.
45 L. Permer and Y. Laligant, *Eur. J. Solid State Inorg. Chem.*, 1997, **34**, 41–52.
46 D. E. Keller, D. C. Koningsberger and B. M. Weckhuysen, *J. Phys. Chem. B*, 2006, **110**, 14313–14325.
47 K. Bhattacharya, S. M. T. Abtab, M. C. Majee, A. Endo and M. Chaudhury, *Inorg. Chem.*, 2014, **53**, 8287–8297.
48 H. Kim, K. M. Kosuda, R. P. van Duyne and P. C. Stair, *Chem. Soc. Rev.*, 2010, **39**, 4820–4844.
49 X. T. Gao, S. R. Bare, J. L. G. Fierro and I. E. Wachs, *J. Phys. Chem. B*, 1999, **103**, 618–629.
50 M. A. Banares and I. E. Wachs, *J. Raman Spectrosc.*, 2002, **33**, 359–380.
51 D. A. Bulushev, S. I. Reshetnikov, L. Kiwi-Minsker and A. Renken, *Appl. Catal., A*, 2001, **220**, 31–39.
52 I. E. Wachs, J. M. Jehng, G. Deo, B. M. Weckhuysen, V. V. Guliants and J. B. Benziger, *Catal. Today*, 1996, **32**, 47–55.
53 D. Goebke, Y. Romanyshyn, S. Guimond, J. M. Sturm, H. Kuhlenbeck, J. Dobler, U. Reinhardt, M. V. Ganduglia-Pirovano, J. Sauer and H. J. Freund, *Angew. Chem., Int. Ed.*, 2009, **48**, 3695–3698.